A comparison of the flowfields and emissions of high-swirl injectors and low-swirl injectors for lean premixed gas turbines

M.R. Johnson[a], D. Littlejohn[a], W.A. Nazeer[b], K.O. Smith[b], R.K. Cheng[a],*

[a] *Environmental Energy Technologies Division, Lawrence Berkeley National Laboratory, Berkeley, CA 94720, USA*
[b] *Advanced Combustion Engineering, Solar Turbines Incorporated, San Diego, CA 92186, USA*

Abstract

A new approach for low emission gas turbines was investigated by modifying a typical production high-swirl injector (HSI) for gas turbine combustors to operate in a novel low-swirl mode (LSI). This LSI ($S = 0.5$) was configured in the laboratory and investigated by particle image velocimetry at firing rates of 9–87 kW ($1 < U_0 < 10$ m/s). It was also tested at simulated gas turbine conditions of 0.08–2.2 MW ($20 < U_0 < 50$ m/s) at elevated combustion inlet temperatures ($230 < T_0 < 430$ °C) and pressures ($6 < P_0 < 15$ atm). The results were compared with those obtained with a HSI ($S = 0.73$). The PIV results show that the flowfields of the LSI are devoid of a large dominant recirculation zone. This is fundamentally different than the strong and large recirculation regions that dominate flowfields of the HSI. Under simulated engine conditions, the LSI has the same operating range as the HSI. Its NO_x emissions were about 60% lower than the HSI, and its CO emissions were comparable. The lack of a strong recirculation zone and the shorter residence time within the LSI may provide an explanation for the NO_x reduction. These results demonstrate that the LSI is a promising solution for attaining an ultra-low emissions target of <5 ppm NO_x (15% O_2) in gas turbines.
© 2004 by the Combustion Institute. Published by Elsevier Inc. All rights reserved.

Keywords: Gas turbines; Lean premixed; Swirl; NO_x; Emissions

1. Introduction

Lean premixed combustion is a proven method to reduce NO_x emissions from land-based gas-turbines. This so-called dry-low-NO_x (DLN) technology has reduced NO_x and CO emissions below 25 and 50 ppm, respectively (corrected to 15% O_2) from engines operating on natural gas [1]. However, with increasingly stringent air quality rules being implemented in US, gas-turbine manufacturers continue to seek new combustion technologies to meet the <5 ppm NO_x (15% O_2) target without having to employ expensive exhaust gas cleanup systems. Attaining such low emission levels requires the DLN combustors to operate at very lean conditions close to the lean blow-off limit (LBO) where gas turbine combustors are highly susceptible to combustion-driven oscillations. There has been much effort to investigate the mechanisms driving combustion instabil-

* Corresponding author. Fax: +1 510 486 7303.
E-mail address: RKCheng@lbl.gov (R.K. Cheng).

PROCI 37

12 August 2004   Disk Used

ARTICLE IN PRESS

No. of Pages 9; 4C:6; DTD = 5.0.1

Chitra (CE) / Jayanthi (TE)

2   *M.R. Johnson et al. / Proceedings of the Combustion Institute xxx (2004) xxx–xxx*

ities and their control [2–5]. Gas turbine manufactures are also developing alternatives to DLN including catalytic combustors and metal fiber injectors. Though effective, these approaches have many engineering issues associated with integration, control, durability, maintenance, and cost that have to be resolved before they can be successfully deployed. Yet another method to further reduce emissions and improve stability (LBO) that has recently been investigated in the laboratory is by H_2 addition [6,7]. In the present work, we are proposing a simpler solution that involves the application of a novel low-swirl flame stabilization method [8–10] to DLN gas turbine injectors.

Typical design of a high-swirl injector (HSI) found in the current DLN gas turbines consists of an annular swirler section with either curved or flat vanes attached to a solid centerbody [3–6,11,12] (Fig. 1 left). Fuel (natural gas) is usually injected through spokes placed just upstream or downstream of each of the vanes or through the vanes themselves. The centerbody acts as a flame anchor by producing a tight toroidal vortex in its wake that entrains and recirculates hot combustion products to continuously ignite the fresh reactants. Under some conditions, a non-premixed pilot flame may also be used to aid stability.

The low-swirl flame stabilization mechanism operates on a different principle. It exploits the turbulent flame speed concept by enabling a detached flame to freely propagate in a divergent flowfield [10,13]. Laboratory low-swirl burner (LSB) has been a very useful experimental configuration for studies of premixed turbulent flame structures. It has low LBO limits and good combustion stability at very lean and highly turbulent conditions [14]. Adaptation of this novel concept to heating equipment has been successful [15] and resulted in commercial LSBs with NO_x emissions below 9 ppm (at 3% O_2). Recently, the validity of this flame stabilization mechanism at high initial temperatures, T_0, and pressures, P_0, has been demonstrated by operating an LSB at 600 °C and 10 atm [8].

To develop a low-swirl injector (LSI) for gas turbines, we explored the feasibility of modifying the existing DLN/HSI hardware into an LSI. If successful, this would bring about significant engineering and economic advantages because the LSI would be compatible to the current engine configurations, and the cost for its adaptation would be
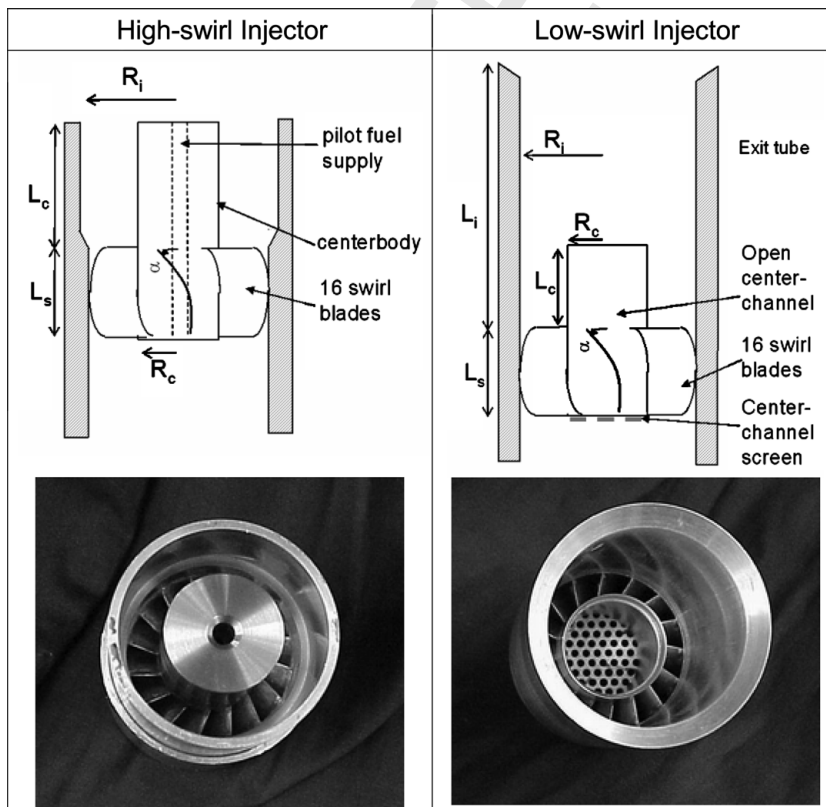

Fig. 1. Schematics and photographs of the HIS (left) and the LSI (right).

PROCI 37

12 August 2004   Disk Used

ARTICLE IN PRESS

No. of Pages 9; 4C:6; DTD = 5.0.1

Chitra (CE) / Jayanthi (TE)

M.R. Johnson et al. | Proceedings of the Combustion Institute xxx (2004) xxx–xxx   3

greatly reduced. The objective of this paper is to compare a conventional HSI with a low-swirl injector derived from the HSI. The two injectors were investigated by laboratory experiments as well as full-scale single injector rig tests at simulated engine conditions.

2. Injector configurations

The main component of the HSI and LSI is a swirler with an outer radius of 3.17 cm. It is sized for 5–7 MW engines and consists of 16 curved vanes attached to the outer surface of a centerbody with $R_c = 2$ cm and a vane angle $\alpha = 42°$ at the exit. The swirler section has a length L_s of 2.8 cm. When configured for HSI (Fig. 1, left), the swirler is fitted with a solid centerbody with a central pilot fuel supply line. This centerbody extends 5.0 cm beyond the swirl vanes ($l_c = 5$ cm) and is flushed with the injector exit. The injector radius, $R_i = 3.47$ cm, is slightly larger than the swirler radius. Except for the absence of a set of fuel injector spokes, this HSI is identical to a production injector. In normal operation, up to 4% of the fuel is injected through a central diffusion flame pilot to ensure flame stability. As this pilot can contribute to the emissions of the HSI, we limited our laboratory studies to the non-piloted cases (the pilot supply line is blocked). For the elevated T_0 and P_0 rig tests, a neutral pilot was used (pilot and injectors have identical stoichiometry).

The swirl number, S, is defined as $S = G_{ang}/G_x R_i$, where G_{ang} is the axial flux of angular momentum, and G_x is the axial flux of linear momentum [16]. In terms of the input flows to the injector:

$$S = \frac{2}{3} \tan \alpha \frac{1 - R^3}{1 - R^2}, \qquad (1)$$

where $\alpha = 42°$ and R is the ratio R_c/R_i. Accordingly, S for the HSI is 0.73. This is within the range of $0.6 < S < 1.6$ used in other fundamental studies [6,11,12].

To configure the swirler for LSI, the solid centerbody is removed to form a centerchannel that allows a portion of the reactants to bypass the swirler. This reproduces the key feature of the LSB swirler described in [15]. A perforated screen is fitted at the entrance of the centerchannel to control the ratio, $m = m_c/m_s$, between the mass flows from the unswirled centerchannel, m_c, and the swirled annulus, m_s, (Fig. 1 right). From [7] a swirl number definition for LSI is:

$$S = \frac{2}{3} \tan \alpha \frac{1 - R^3}{1 - R^2 + m^2((1/R^2) - 1)^2 R^2}. \qquad (2)$$

Here R is 0.63, and screens with different blockage ratios can be used to vary m, and hence S. Based on our experience in configuring LSBs, we developed a guideline of $0.4 < S < 0.55$ and $1 < l_i < 1.5 D_i$, where D_i is the diameter of the injector at the exit. For the LSI, we used an exit tube length of $l_i = 9.5$ cm with a 45° tapered edge and centerbody screens with 73–50% blockages. To determine the optimum LSI configuration, we tested the LSI with these screens at different equivalence ratios ϕ and bulk flow velocities of $U_0 < 5$ m/s. Using the LBO and flame position as the criteria, a 58% blockage screen was selected. To determine flow split m for this LSI, the drag coefficients for the screen and for the swirl annulus were determined separately. From the drag ratio, m for the LSI was 0.3, and the swirl number was $S = 0.5$.

3. Diagnostics and experimental systems

Flowfield information for the HSI and LSI at STP was obtained using particle imaging velocimetry (PIV). The PIV system consists of a New Wave Solo PIV laser with double 120 mJ pulses at 532 nm and a Kodak/Red Lake ES 4.0 digital camera with 2048×2048 pixel resolution. The optics captured a field of view of approximately $13 \text{ cm} \times 13 \text{ cm}$ covering the nearfield as well as the farfield of the flames with 0.065 mm/pixel resolution. A cyclone type particle seeder seeded the air flow with 0.6-0.8 μm Al_2O_3 particles, which should track velocity fluctuations up to 10 kHz [17].

Data acquisition and analysis were performed using software developed by Wernet [18]. Because of the complex and 3D nature of the swirling flowfield, care had to be taken to optimize interframe timing, camera aperature setting, light-sheet thickness, and seed density to ensure high data fidelity. Using a portion of the light sheet with approximately 1.1 mm thickness (away from the 0.3 mm waist produced by the 450 mm spherical lens) and a short interframe time (35 μs) helped to freeze the out-of-plane motion of seed particles. Sets of 448 image pairs were recorded for each experiment corresponding to the minimum criterion (450 image pairs) required to produce stable mean and rms velocity. The PIV data were processed using 64×64 pixels cross-correlation interrogation regions with 50% overlap. This rendered a spatial resolution of approximately 2 mm. The velocity statistics were checked to ensure that significant spatial bias or "peak-locking" was not taking place.

For the PIV and LBO investigations, the injectors were mounted vertically on top of a cylindrical settling chamber connected through a converging nozzle and fired into ambient air without an enclosure. Compressed air enters at the

PROCI 37

12 August 2004   Disk Used

ARTICLE IN PRESS

No. of Pages 9; 4C:6; DTD = 5.0.1

Chitra (CE) / Jayanthi (TE)

4   *M.R. Johnson et al. | Proceedings of the Combustion Institute xxx (2004) xxx–xxx*

base of the chamber and is monitored by a turbine meter. Fuel (research grade methane) is injected in the air supply duct to ensure a homogeneous mixture for the injectors. Both the fuel and the PIV seeder flows are controlled by electronic mass flow controllers. The experimental setup is controlled by a PC and affords a maximum flow rate of 2000 LPM.

For the rig tests, two different facilities at solar turbines were used. A "quartz tube rig" that simulates the enclosure environment of a gas turbine combustor is used for atmospheric testing. The injectors fire vertically into a quartz cylinder of 45 cm in length and 20 cm in diameter that affords full view of the flame. There is no constriction at the exit of the cylinder where an emission sampling probe is placed centrally. This facility can supply preheated air at temperatures up to 450 °C. For the quartz tube rig tests, the LSI was mounted with two different proprietary premixers. One produces reactants with ±3% uniformity, and the other ±10%.

A high-pressure "combustor rig" provides a full simulation of elevated T_0 and P_0 environment in a gas turbine. It is a horizontal stainless steel cylindrical chamber housing an assembly consisting of an injector and a combustor liner. Combustor pressure and airflow rates are controlled by a pressure regulating valve upstream and a back-pressure valve downstream of the combustor. The chamber has a small quartz window offering a side view of the flame. Instrumentation allows monitoring of the air and fuel flows, inlet air temperature and pressure, combustion fluctuation spectrum, combustor wall temperatures, combustor pressure drop, and exhaust gas composition (CO, CO_2, NO_x, O_2, and unburned hydrocarbons). The HSI and LSI were fitted to a "film-cooled liner," a standard configuration for single injector testing. The liner forms a can type combustor 45.7 cm long and 20.3 cm ID. It is constructed of a 2 mm thick Hastelloy × sheet metal. As a prerequisite for testing with this liner, the pressure drop across the LSI was measured and shown to have 50% less pressure drop than the HSI. This feature can be a potential efficiency gain when applied to engines. All the HSI and LSI combustor rig tests were performed with natural gas. For the LSI, $a \pm 10\%$ premixer was used. The HSI utilized a multi-spoke fuel injection assembly typical of those in production engines.

4. Results

4.1. Laboratory experiments

4.1.1. Flame stability and lean blow-off

Flame stability and LBO were determined by maintaining a constant volumetric flow rate, Q, of 300–1880 LPM and incrementally reducing the fuel flow until the flame became unstable and eventually blew off. Fig. 2 shows a comparison of the results obtained for HSI and LSI plotted against the bulk velocity $U_0 = Q/A_i$, where A_i is the open area of the injectors. Also shown are the results reported by Schefer et al. [6] for a smaller ($R_i = 2.05$ cm) high-swirl burner (HSB) with estimated $S = 0.82$. The HSI becomes visibly unstable (i.e., intermittent local flame detachment off the centerbody) at $0.62 < \phi < 0.65$, and LBO occurs at $0.55 < \phi < 0.6$. Both boundaries show a moderate increasing trend with U_0. For the LSI, however, an unstable boundary cannot be determined because the lifted flame (see Fig. 3 top right) remains stationary without shifting downstream as ϕ is reduced. Towards LBO, the flame becomes visibly weaker and smaller, and eventually disappears. The LSI LBO limit of $0.5 < \phi < 0.52$ is lower than the HSI LBO and seems relatively insensitive to U_0 in the range 3 m/s $< U_0$. For the HSB of [6], instability occurs at much lower ϕ than our HSI, and its LBO limits matches that of LSI at $U_0 = 9$ m/s. The better performance of this HSB may be due to enclosure effects that can provide some heat retention to promote a more stable and leaner flame.

4.1.2. PIV measurement

Table 1 shows the conditions for the PIV experiments for HSI and LSI. Although U_0 of these laboratory experiments are low compared to U_0 of up to 50 m/s in engines, they are within the typical range for hardware development. The flames in Fig. 3 ($\phi = 0.8$) illustrate the basic differences of the HSI and LSI operational modes. The oblique HSI flame is attached to the rim of the centerbody while LSI flame is bowl shaped and fully detached. In the raw PIV images, contrast between the Mie scattering intensities in the reac-
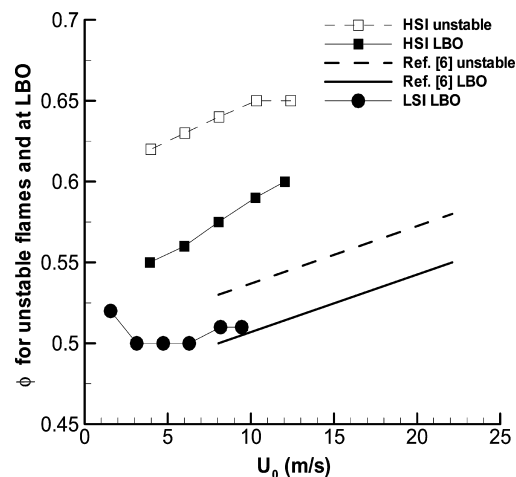
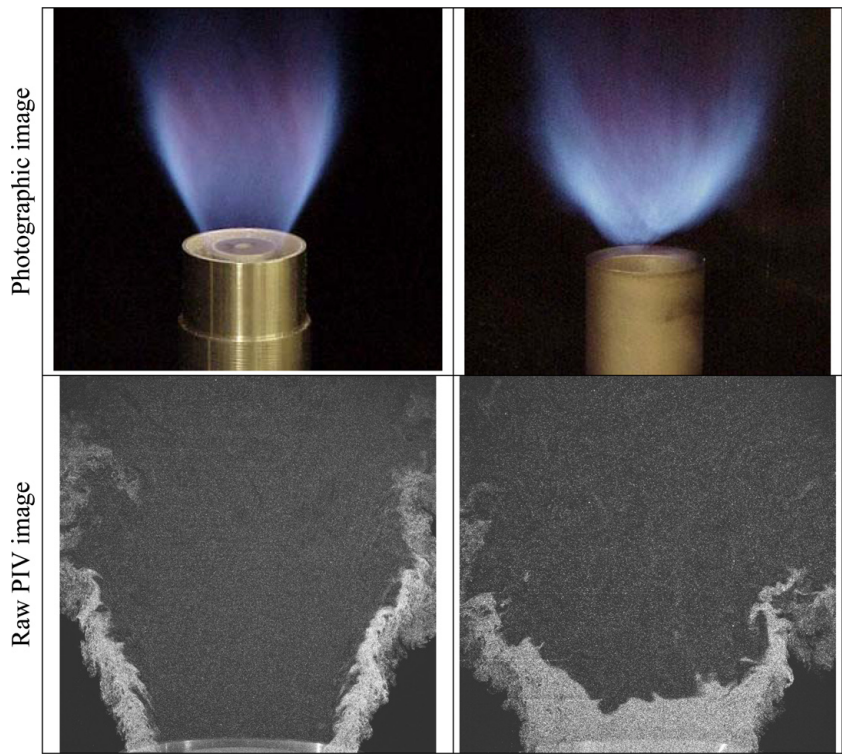Fig. 2. Flame instability and lean blow-off limits at STP.

PROCI 37

12 August 2004   Disk Used

ARTICLE IN PRESS

No. of Pages 9; 4C:6; DTD = 5.0.1

Chitra (CE) / Jayanthi (TE)

M.R. Johnson et al. / Proceedings of the Combustion Institute xxx (2004) xxx–xxx   5

Fig. 3. Direct and PIV images of flames generated by HSI (left) and LSI (right).

Table 1
Laboratory experiments at STP

Run	ϕ	S	Reactant flow		U_0 (m/s)	Heat release (kW)
			(LPM)	(g/s)		
HSI-LE0	0.0	0.73	1817	36.5	12.0	0.0
HSI-LE1	0.7	0.73	1816	35.3	12.0	76.9
HSI-LE2	0.8	0.73	1819	35.2	12.0	87.0
LSI-LE0	0.0	0.5	1819	36.5	9.6	0.0
LSI-LE1	0.7	0.5	1817	35.4	9.6	76.9
LSI-LE2	0.8	0.5	1814	35.1	9.6	86.8

tants and the products outlines the flame fronts and show that the HSI produces finer flame wrinkles than the LSI.

Fig. 4 shows the mean velocity vectors and the contours of 2 D turbulent kinetic energy, $q' = \frac{1}{2}\sqrt{u'^2 + v'^2}$ measured in the HSI where u' and v' are the rms fluctuation velocities in the axial and radial directions, respectively. The dominant feature of all three cases is a large recirculation zone as illustrated by the flow reversal regions downstream of the centerbody at $\pm r/D = 0.31$. Combustion heat release has the effect of weakening the reversed flow at the centerline and also slightly shortens as well as broadens the recircula-

tion zone. These are the same trends reported in [12]. The swirling flows above the annulus are characterized by axial velocity U reaching up to 16 m/s in the nearfield of the non-reacting flow (Fig. 4A) and up to $\approx$18.5 m/s for the reacting cases (Figs. 4B and C). It is within these high velocity and shear regions (high values of the cross-correlation $\overline{uv}$ computed but not shown here) at the edge of the recirculation zones where the HSI flame stabilizes. The q' contours in the backgrounds of Fig. 4 illustrate that the high turbulence levels are confined to the shear regions. Within the non-reacting flow, u' and v' reach up to 6 and 3.5 m/s, respectively. For the two reacting

PROCI 37

12 August 2004   Disk Used

ARTICLE IN PRESS

No. of Pages 9; 4C:6; DTD = 5.0.1

Chitra (CE) / Jayanthi (TE)

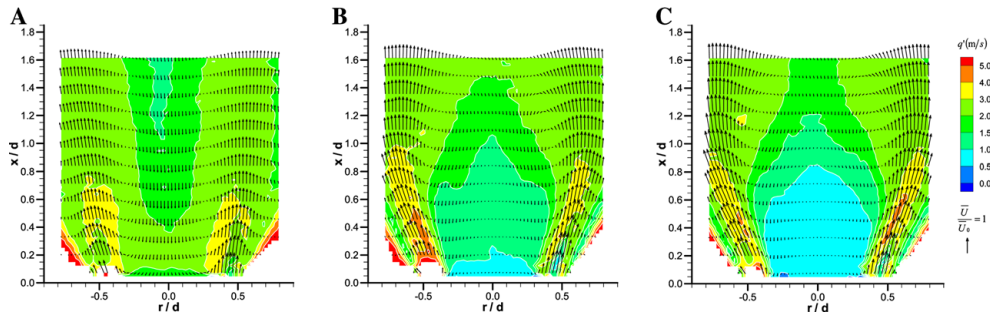6   M.R. Johnson et al. / Proceedings of the Combustion Institute xxx (2004) xxx–xxx

Fig. 4. Mean velocity vectors superimposed on contours of 2D turbulent kinetic energy measured in a HSI. For all cases Q = 1818 LPM (U_0 = 12.0 m/s). (A) ϕ = 0 (non-reacting); (B) ϕ = 0.7; and (C) ϕ = 0.8.

331 cases, u' and v' further increase to 7 and 4.5 m/s,
332 respectively. Such increases within the flame zones
333 are consistent with contributions from the com-
334 bustion induced mean velocity jumps across the
335 oblique wrinkled flame fronts. In contrast, the tur-
336 bulence levels inside the recirculation zones de-
337 crease with increasing ϕ. This seems to be
338 caused by a weakening of the reciruation zone
339 (see below) combined with an increase in viscosity
340 in the hot products.
341   The flowfields of the LSI shown in Fig. 5 are
342 devoid of strong recirculation. For the non-react-
343 ing flow (Fig. 5A), the vectors in the nearfield
344 (0.4 < x/D) show a slightly divergent central re-
345 gion (−0.25 < r/D < 0.25) where the velocity dis-
346 tribution is relatively flat. Similar features have
347 been reported previously for a LSB that uses an
348 air-jet swirler [13]. This central region decelerates
349 with increasing x/D dipping to −0.2 m/s at $x/$
350 D = 1 and then reverting back to positive. Com-
351 pared to Fig. 4A, the LSI recirculation zone is
352 much smaller and weaker. In the swirl annulus re-
353 gion (r/D > 0.31), both mean and rms velocities
354 are lower than those found in the non-reacting
355 HSI. Peak U, u', and v' are in the order of 12, 2,
356 and 3 m/s, respectively.
357   For the reacting LSI cases (Figs. 5B and C),
358 their flow features below the leading edges of the

359 flame brushes (x/D < 0.28 for ϕ = 0.7 and $x/$
360 D < 0.2 for ϕ = 0.8) are similar to the non-react-
361 ing case. Compared to the analogous flame region
362 of the HSI, the central region where the LSI flame
363 stabilizes and propagates has relatively lower
364 velocities, turbulence intensities, and shear stres-
365 ses (2.1 < U < 2.5 m/s, 0.65 < u' < 0.7 m/s, 0.3
366 < v' < 0.35 m/s, and $\overline{uv}$ ≈ 0). Again, this demon-
367 strates that the low-swirl flame stabilization mech-
368 anism is based on the concept of a freely
369 propagating turbulent flame in a divergent flow
370 instead of the concept of hot products entrain-
371 ment. In Fig. 5B, close examination of the velocity
372 vectors within the central region of LSI ϕ = 0.7
373 case shows slight combustion induced acceleration
374 within the flame and less rapid velocity decay
375 downstream. Consequently, the weak flow recir-
376 culation zone is pushed downstream to $x/$
377 D > 1.5. With increased heat release at ϕ = 0.8
378 (Fig. 5C), flow reversal is not found. The q' con-
379 tours of Fig. 5A–C also show a decrease in turbu-
380 lence intensities throughout the central region as
      ϕ is increased.   ς

382 4.1.3. Structure and strength of HSI and LSI
383 recirculation zones
384   As reported in [12], the instantaneous flowfield
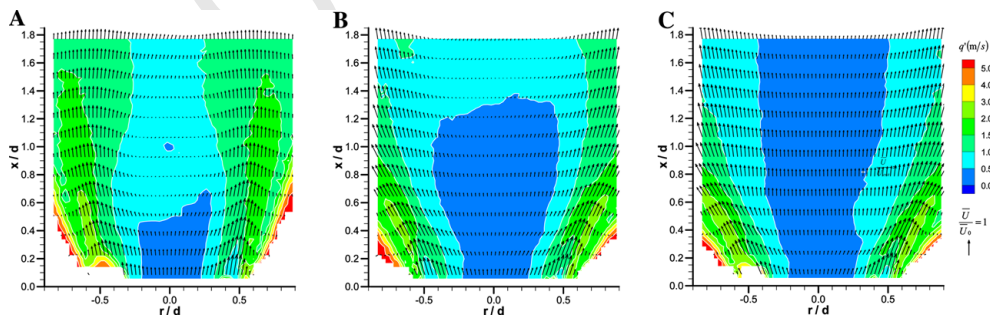385 of the recirculation zone in a high-swirl burner is

Fig. 5. Mean velocity vectors superimposed on contours of 2D turbulent kinetic energy measured in a LSI. For all cases it Q = 1818 LPM (U_0 = 9.6 m/s). (A) ϕ = 0 (non-reacting); (B) ϕ = 0.7; and (C) ϕ = 0.8.

PROCI 37

12 August 2004   Disk Used

ARTICLE IN PRESS

No. of Pages 9; 4C:6; DTD = 5.0.1

Chitra (CE) / Jayanthi (TE)

M.R. Johnson et al. | Proceedings of the Combustion Institute xxx (2004) xxx–xxx   7

very complex and does not resemble the large and coherent vortex structure suggested by the mean velocities. Here, the complex flowfield structures in HSI at $\phi = 0.7$ were examined by instantaneous $U = 0$ contours at over 20 random instances. This is a condition close to the unstable limit, and we found that the flow reversal regions grow and shrink and sometimes detach from the center-body. Such an occurrence may trigger flame detachment in a weaker flame. Conversely, the recirculation zone found in LSI at $\phi = 0.7$ is far downstream from the flame and is much smaller and weaker having little influence on flame stability.

To compare the recirculation strengths, we estimated the recirculated mass flow ratio (M_r/M_0) [11,19] by assuming that the recirculated and reactants fluids maintained density ratios ρ_p/ρ_r of 1, 0.162, and 0.15, respectively, for the $\phi = 0$, 0.7, and 0.8 cases. These values for ρ_p/ρ_r were obtained by invoking the adiabatic flame temperature without correcting for radiative heat loss and other possible cooling effects due to entrain-

ment. The results are compared in Fig. 6. For the non-reacting cases, M_r/M_0 in HSI is the same as that of a disk flame stabilizer reported in [19]. With combustion, M_r/M_0 in the two HSI flames is reduced by a factor of 3 to about the same level as reported in [11] for a non-premixed flame with $S = 0.9$. In contrast, values of M_r/M_0 in the LSI are significantly lower. At $\phi = 0$, M_r/M_0 is 40 times lower than in the HSI and at $\phi = 0.7$, the reduction is by an order of magnitude. These results clearly show that the weak recirculation zones generated by LSI are not relevant to the flame stabilization mechanism as discussed in [14]. Moreover, the recirculation can be reduced or prevented with increased heat release from the flame.

4.2. Rig tests

The rig tests were performed to verify the operability of the LSI at typical engine conditions, and to determine its effectiveness in lowering emissions. Table 2 shows the experimental matrix. LSI-QR1 and -QR2 were performed with pre-heated air in the quartz tube rig. Completions of the quart tube rig tests gave confidence to proceed to combustor rig tests LSI-CR1 to -CR5. HSI-CR1, with a neutral gas pilot to produce a purely premixed flame, was selected from a vast HSI database.

Visual observation during LSI-QR1 and LSI-QR2 showed that the locations of the flames were not very sensitive to U_0, ϕ, and T_0. LSI-QR1 and LSI-QR2 at ±3% and ±10% mixture uniformity also show that stoichiometry fluctuations have minimal effects on the overall flame behavior and characteristics. The combustor rig tests LSI-RT1 to -RT5 covered partial and full load conditions of 5–7 MW engines and showed that the operating range of the LSI is fully compatible with that of the HSI. Throughout these tests, there were no indications of shifting in flame positions or flashback. No excessive acoustic amplitudes were observed, and peak rms acoustics pressures were generally below the allowable 3.4 kPa established for production engines.
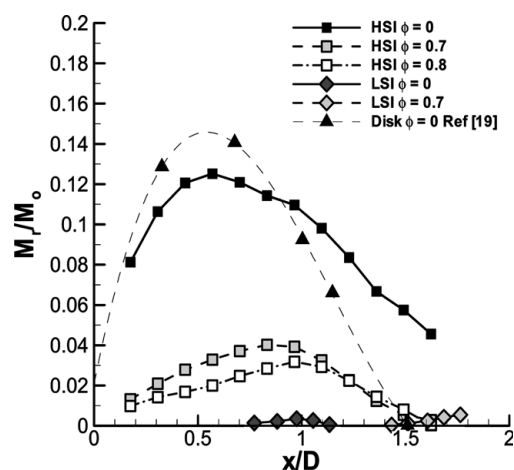

Fig. 6. Recirculation zone strength as characterized by the normalized mass flux of fluid in the negative axial direction.

Table 2
Rig-test conditions

Run	ϕ	Air flow (kg/s)	Fuel flow (kg/h)	T_0 (°C)	P_0 (atm)	U_0 (m/s)	Heat release (MW)
LSI-QR1	0.5–0.63	0.05–0.07	5.5–9.3	360–370	1	24–34	0.08–0.14
LSI-QR2	0.48–0.63	0.065–0.09	7.3–12	375–380	1	32–44	0.1–0.18
LSI-CR1	0.67–0.7	0.44–0.5	63–76	230	6	30–39	1–1.1
LSI-CR2	0.64–0.76	0.8	111–130	230	11	29–31	1.7–2.0
LSI-CR3	0.55–0.67	1–1.16	96–112	341	11	36–40	1.4–1.7
LSI-CR4	0.53–0.7	1–1.16	120–163	370	12	45–52	1.8–2.5
LSI-CR5	0.51	1.33	147	430	15	48	2.2
HSI-CR1	0.53–0.72	0.71–0.72	80–111	360	11	31–32	1.2–1.7

PROCI 37

12 August 2004   Disk Used

ARTICLE IN PRESS

No. of Pages 9; 4C:6; DTD = 5.0.1

Chitra (CE) / Jayanthi (TE)

8   M.R. Johnson et al. / Proceedings of the Combustion Institute xxx (2004) xxx–xxx

Fig. 7 shows NO_x and CO emissions from the LSI QR and CR tests compared with the emissions of HSI-CR1. Due to the variation in T_0 and P_0, NO_x emissions data expressed in terms of ϕ have significant scatter. After examining the data against various experimental parameters, the most consistent trend was found when NO_x data were plotted against the theoretical adiabatic flame temperature T_{ad} as in Fig. 7A. All the LSI NO_x data collapse onto a narrow band that crosses the 5 ppm threshold at $T_{ad} < 1920$ K. A lack of differences between the NO_x emissions of LSI-QR1 and LSI-QR2 also indicate that a tight control on mixture homogeneity is not critical. In comparison, NO_x emissions of HSI-CR1 are generally higher and only approach the 5 ppm NO_x threshold. Though the HSI-CR1 NO_x emissions may be slightly elevated due to its utilization of a production fuel-spoke injector and a neutral pilot, the over 2.5 times difference between the NO_x emissions of LSI and HSI still represents a substantial improvement. These results also imply that the LSI can operate farther away from LBO (higher T_{ad}) so that it may be less prone to combustion oscillation. Although the CO emissions in Fig. 7b do not show a consistent trend, they are all within acceptable limits. CO emissions from the quartz-rig tests are between 10 and 20 ppm while all but one of the test data from the high temperature

and pressure LSI rig tests are below 5 ppm. Therefore, the LSI does not entail compromising CO for the sake of lowering NO_x.

The emissions from LSI rig tests are very encouraging and show that the LSI has the potential to bring about a significant reduction in NO_x emissions from DLN gas turbines. In fact, the NO_x emissions of Fig. 7A are comparable to those from a more complex and less durable catalytic combustor. Despite the complexity of the NO_x formation mechanisms, differences in the HSI and LSI flowfields may provide an explanation for their NO_x emission characteristics. Many recent studies on high-swirl burners and injectors have shown a relationship between NO_x emissions and swirl intensity as well as the residence time within the recirculation zone. Schmittel et al. [11] concluded that decreasing the residence time helps to lower NO_x. Our experience in adapting low-swirl burner for industrial applications also provides additional empirical support to this notion. From the PIV results, it is clear that without a strong recirculation zone with a large recirculated mass, the residence time of the hot products in a LSI should be much shorter than in a HSI. This may be the key to better understand the NO_x evolutionary paths in the two injectors.

These rig tests for the first time show the validity of the low-swirl flame stabilization method for a wide range of ϕ at elevated T_0 and P_0. More significantly, they also confirm its effectiveness in lowering gas turbine emissions and provide the impetus for continuing the development of LSI prototypes for testing in gas turbine engines. In parallel, we plan to conduct laboratory experiments to gain a better understanding of the fundamental processes that enable the low-swirl flame stabilization method to maintain flame stability and low emissions, and also to assist in the development of theories and computational methods.

5. Conclusions

A high-swirl injector for DLN gas turbine has been converted to operate in a novel low-swirl stabilization mode. The lean blow off limits and flowfields of this low-swirl injector ($S = 0.5$) were investigated at STP in the laboratory at 9–87 kW ($1 < U_0 < 10$ m/s) by PIV. It was also evaluated in high temperature ($230 < T_0$ 430 °C) and high pressure ($6 < P_0 < 15$ atm) environments at 0.08–2.2 MW ($20 < U_0 < 50$ m/s). The results were compared with those obtained with a conventional high-swirl injector of $S = 0.73$.

Analysis of the PIV data has shown that the flow generated by the LSI is devoid of a large dominant strong recirculation zone. Instead the non-reacting LSI flow generated a small and very weak recirculation in the farfield that further weakened and disappeared in the presence of
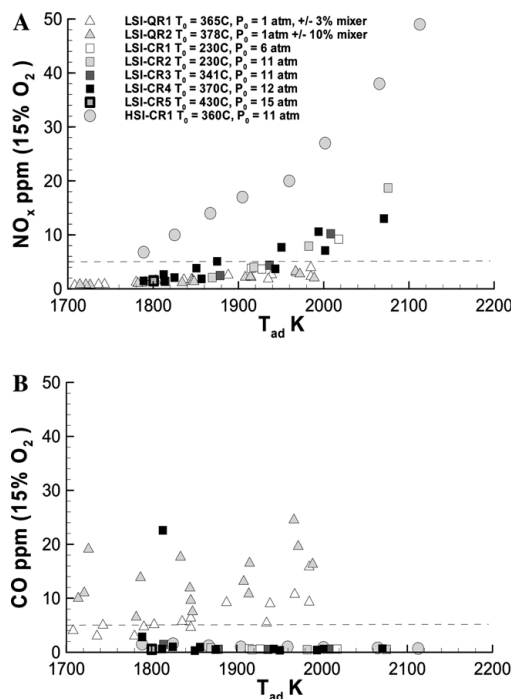

Fig. 7. Rig test emissions measurements for LSI and HSI at atmospheric and high pressure conditions over a range of air preheat temperatures.

PROCI 37

12 August 2004   Disk Used

ARTICLE IN PRESS

No. of Pages 9; 4C:6; DTD = 5.0.1

Chitra (CE) / Jayanthi (TE)

M.R. Johnson et al. | Proceedings of the Combustion Institute xxx (2004) xxx–xxx   9

combustion. This is fundamentally different than the flowfields of the HSI that are dominated by strong and large recirculation regions. Combustion tends to enlarge the HSI recirculation zones and generate complex flow structures within them.

The HSI and LSI have similar operating ranges. When tested in a simulated gas turbine environment up to full load conditions of typical 5–7 MW engines, the flames produced by the LSI remained stationary despite changes in ϕ, T_0, P_0, and U_0. The LSI emits NO_x levels about 60% lower than from the HSI and has no effect on CO. These results strongly suggest that the LSI is a very promising simple and economic solution for gas turbines to attain an ultra-low emissions target of <5 ppm NO_x.

Acknowledgments

References

[1] D.C. Rawlins, *SoLo NO_x Combustion Systems Update*, Turbomachinery Tech. Seminar, Solar Turbines, 1995.

[2] S. Candel, *Proc. Combust. Inst.* 29 (2002) 1–28.

[3] T. Lieuwen, Y. Neumeier, B.T. Zinn, *Combust. Sci. Technol.* 135 (1–6) (1998) 193–211.

[4] G.A. Richards, M.C. Janus, *Trans. ASME* 120 (2) (1998) 294–302.

[5] S.-Y. Lee, S. Seo, J.C. Broda, R.J. Santoro, *Proc. Combust. Inst.* 28 (2000) 775–782.

[6] R.W. Schefer, D.M. Wicksall, A.K. Agrawal, *Proc. Combust. Inst.* 29 (2002) 843–851.

[7] D. Littlejohn, M.J. Majeski, S. Tonse, C. Castaldini, R.K. Cheng, *Proc. Combust. Inst.* 29 (2) (2002) 1115–1121.

[8] R.K. Cheng, D.A. Schmidt, L. Arellano, K.O. Smith, in: *IJPGC2001*, New Orleans, 2001.

[9] D.T. Yegian, R.K. Cheng, *Combust. Sci. Technol.* 139 (1–6) (1998) 207–227.

[10] C.K. Chan, K.S. Lau, W.K. Chin, R.K. Cheng, *Proc. Combust. Inst.* 24 (1992) 511–518.

[11] P. Schmittel, B. Gunther, B. Lenze, W. Leuckel, H. Bockhorn, *Proc. Combust. Inst.* 28 (1) (2000) 303–309.

[12] J. Ji, J.P. Gore, *Proc. Combust. Inst.* (2002) 861–867.

[13] R.K. Cheng, *Comb. Flame* 101 (1–2) (1995) 1–14.

[14] T. Plessing, C. Kortschik, M.S. Mansour, N. Peters, R.K. Cheng, *Proc. Combust. Inst.* 28 (2000) 359–366.

[15] R.K. Cheng, D.T. Yegian, M.M. Miyasato, G.S. Samuelsen, R. Pellizzari, P. Loftus, C. Benson, *Proc. Combust. Inst.* 28 (2000) 1305–1313.

[16] T.C. Claypole, N. Syred, *Proc. Combust. Inst.* 18 (1981) 81–89.

[17] A. Mellings, *Meas. Sci. Tech.* 8 (1997) 1406–1416.

[18] M.P. Wernet, in: *18th International Congress on Instrumentation for Aerospace Simulation Facilities*, Toulouse, France, 1999.

[19] T.W. Davies, J.M. Beer, *Proc. Combust. Inst.* 13 (1971) 631–638.